



Geostatistical simulation to map the spatial heterogeneity of geomechanical parameters: A case study with rock mass rating



Marisa Pinheiro ^{a,*}, Javier Vallejos ^{b,c}, Tiago Miranda ^a, Xavier Emery ^{b,c}

^a ISISE, University of Minho, Azurém, 4800-058 Guimarães, Portugal

^b Department of Mining Engineering, University of Chile, Avenida Tupper, 2069 Santiago, Chile

^c Advanced Mining Technology Center, University of Chile, Avenida Beauchef, 850, Santiago, Chile

ARTICLE INFO

Article history:

Received 1 August 2015

Received in revised form 8 March 2016

Accepted 14 March 2016

Available online 17 March 2016

Keywords:

Rock Mass Rating

Rock mechanics

Geostatistical simulation

Spatial heterogeneity

Spatial uncertainty

ABSTRACT

A better characterization of complex rock masses is essential in geotechnical engineering, as the empirical systems widely used for this purpose have significant limitations and do not provide adequate answers for risk analysis. Geostatistics offers a set of tools that allow not only predicting the rock mass properties, but also mapping their heterogeneity at different spatial scales and quantifying the uncertainty in their actual values. In this paper, two geostatistical approaches are compared for modeling the Rock Mass Rating (RMR), which is used to geomechanically characterize the rock mass in geotechnical works. The first approach consists of the direct simulation of the RMR values, based on a Gaussian spatial random field model. In contrast, the second approach uses the truncated Gaussian model to separately simulate the individual parameters of the RMR, which subsequently are summed to obtain the final RMR value. The computation time, practical implementation, level of details and post-processing outputs that can be obtained from both approaches are analyzed. Besides the RMR mapping and associated uncertainty, the deformation modulus is subsequently obtained based on these maps together with empirical expressions.

© 2016 Elsevier B.V. All rights reserved.

1. Introduction

In the current practice of geotechnical works design, the geomechanical parameters of the rock formations are set based on campaigns of in situ and laboratory characterization works and tests. According to the results of these campaigns, a geotechnical zoning is established and a set of geomechanical parameters is assigned to each zone. This is a highly subjective exercise, but its output is of utmost importance for the next stages of geotechnical design. However, this approach does not properly account for the intrinsic spatial variability and high heterogeneities that can be found in many rock masses, which can have a significant impact on the structure behavior. In this sense, there is a lack of an approach that allows reducing the subjectivity of geotechnical zoning and that explicitly considers the spatial variability and heterogeneities many times present in rock masses.

The recourse to geostatistical models can be a mean to foster the development of such an approach. Indeed, in these models, the geomechanical parameters are viewed as outcomes (realizations) of spatial random fields, the properties of which can be inferred from the available in situ measurements and laboratory tests. Kriging techniques (Matheron, 1971) can be used to predict the values of the parameters of interest at any specific location, based on the information available at

neighboring locations and on the spatial correlation structure of the underlying random fields. These techniques aim to minimize the expected squared error between predicted and true values, but, in return, they provide over-smoothed maps that do not reflect the actual variability of the true parameters. To avoid this drawback, conditional simulation techniques have been developed to construct numerical models that reproduce the spatial variability at all scales and allow a better understanding of the rock mass heterogeneities (Journel, 1974; Chilès and Delfiner, 2012). Unlike kriging that provides a single prediction for each parameter of interest, simulation yields as many case scenarios as desired, which are helpful to assess the uncertainty in the actual (unknown) parameter values at any specific location or jointly over several locations.

Numerous authors already applied geostatistics to estimate or to simulate properties such as lithology faces (Rosenbaum et al., 1997), Rock Quality Designation (RQD) (Esfahani and Asghari, 2013; Ozturk and Simdi, 2014; Ozturk and Nasuf, 2002), Rock Mass Rating (RMR) (Ryu et al., 2003; You, 2003; Oh et al., 2004; Stavropoulou et al., 2007; Exadaktylos and Stavropoulou, 2008; Jeon et al., 2009; Egaña and Ortiz, 2013; Ferrari et al., 2014), joint frequency (Ellefmo and Eidsvik, 2009) or Geological Strength Index (GSI) (Ozturk and Simdi, 2014; Deisman et al., 2013).

Hereunder, the system used for simulation is the Rock Mass Rating (RMR) proposed by Bieniawski (1989). This system allows classifying the rock mass in five classes (very good, good, fair, poor, very poor) using a continuous scale that varies from 0 to 100 obtained after weighting six individual parameters regarding the rock mass and its

* Corresponding author.

E-mail address: marisamotapinho@gmail.com (M. Pinheiro).

discontinuities. The referred parameters are: a) Uniaxial compressive strength of rock material (P1); b) RQD (P2); c) Discontinuity spacing (P3); d) Condition of discontinuities (P4); e) Groundwater conditions (P5); f) Orientation of discontinuities (P6). In this work, the sixth parameter (P6) will not be used because it does not depend only on the characteristics of the rock discontinuities but also on their relation with the structure and this is unknown. The RMR under consideration is therefore the so-called basic RMR, which is obtained considering only the contribution of parameters P1 to P5.

The next section presents two geostatistical approaches to simulate the RMR, depending on whether one considers that the properties are measured on a continuous quantitative scale or on a discrete scale. In the first approach, the most straightforward and usual one, RMR is viewed as a variable measured on a continuous scale (from 0 to 100) and is directly simulated with a multivariate Gaussian algorithm. In contrast, the second approach is more complete, as each one of the five parameters (P1 to P5) is simulated and the results are then summed to obtain the final mapping of RMR. A novelty of this second approach with respect to previous works is the fact that the underlying parameters are considered as variables measured on a discrete scale, which better suits their nature as a ranking and not as a continuous value, and that a specific geostatistical model (truncated Gaussian model) is used for the purpose of simulation. In Section 3, both approaches are applied to a case study and compared in terms of implementation facility, accuracy and level of detail provided in simulating the spatial distribution of RMR. Finally the simulated RMR is converted into deformation modulus (E_m) using empirical formulae.

2. Geostatistical simulation of RMR

2.1. First approach: direct simulation of RMR

In this approach, the RMR is viewed as a variable that continuously varies from 0 to 100 and is simulated directly (Fig. 1a). To this end, the multi-Gaussian random field model is used, through the following steps (Chilès and Delfiner, 2012):

- 1) First, a representative distribution of the RMR values is calculated, by weighting each data depending on the geometrical configuration of

the data locations. This procedure aims at down-weighting the data that are spatially clustered, which contain redundant information (Deutsch and Journel, 1998). In case of a regular sampling design, the data can be assigned the same weights.

- 2) The RMR data are then transformed into data with a standard Gaussian distribution, accounting for the previously calculated declustering weights. These transformed data are associated with a parent second-order stationary Gaussian random field, which is fully characterized by its auto-correlation function or, equivalently, by its variogram (Lantuéjoul, 2002).
- 3) The experimental variogram of the Gaussian data is computed and subsequently fitted with a theoretical model. At this stage, the study can be performed in one or more directions of space, in order to identify a possible anisotropy and to better understand the spatial behavior of the data.
- 4) A Gaussian random field is then simulated at the target locations, conditionally to the available data (i.e., such that the values simulated at the data locations match the data values). In the present case the turning bands algorithm (Emery and Lantuéjoul, 2006) is used for simulation.
- 5) The simulated Gaussian values are back-transformed to the original scale (RMR).

Similar approaches, which differ in the specific simulation algorithm used at step (4), have been proposed by Ryu et al. (2003); Jeon et al. (2009); Egaña and Ortiz (2013) and Ferrari et al. (2014), among others, for the spatial prediction of RMR and for uncertainty quantification.

2.2. Second approach: simulation of underlying parameters

The second approach is more innovative and consists in simulating all five parameters assigned with their ratings, viewed as discrete variables (i.e., they only assume integer values). The sum of the simulated parameters gives the final value for RMR.

For the parameter simulation, the truncated Gaussian model (Armstrong et al., 2011) is used, which relies on the truncation of

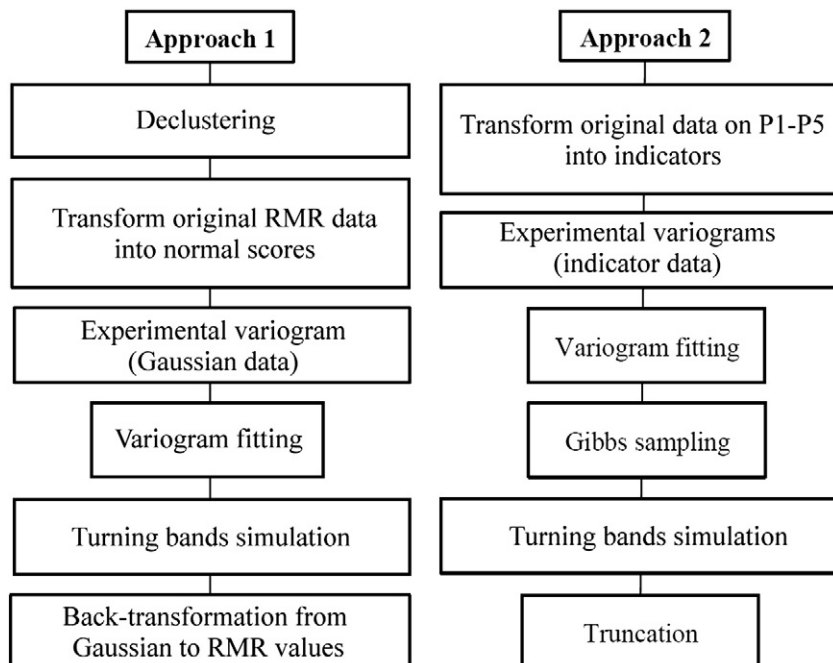


Fig. 1. Flow charts for simulation under the multi-Gaussian model (Approach 1) (a) and the truncated Gaussian model (Approach 2) (b).

second-order stationary Gaussian random fields. The application of this model is carried out through the following steps (Fig. 1b):

- 1) First, the original data are transformed into class-indicator data, i.e., data that take the value 0 or 1 depending on each parameter score.
- 2) For each individual parameter, a set of truncation thresholds is defined, which allows the proportion of each class to be reproduced by the simulation (Armstrong et al., 2011).
- 3) Given the experimental variograms of the class-indicator data, a variogram can be calculated for the underlying Gaussian random field associated with each parameter, based on the existing relationships between the indicator and Gaussian variograms (Emery and Cornejo, 2010). The Gaussian variograms so obtained can be fitted with theoretical models.
- 4) The class-indicator data are then transformed into simulated Gaussian data, using an iterative algorithm known as the Gibbs sampler (Armstrong et al., 2011; Lantuéjoul, 2002).
- 5) The Gaussian random fields are simulated at the target locations, conditionally to the Gaussian values obtained at the previous step, and are truncated in order to get back to simulated class-indicator values. As for the first approach, the turning bands algorithm is used for the simulation of Gaussian fields.
- 6) The indicators are converted into the underlying parameters and finally into RMR values.

3. Case study

The two previous approaches are now applied to a case study in order to map the RMR in an epithermal gold deposit located in the “Cordillera de Los Andes”, region of Atacama, northern Chile, and surveyed through a set of exploration boreholes. The regional geology of the area is characterized by a group of intrusive, volcanic and sedimentary rocks, affected by fault zones that control the mineralization, allowing the identification of four main lithological units of sedimentary rocks.

The available data comprise 3969 samples obtained from boreholes with a horizontal spacing of 40 m × 40 m and depths ranging from 96 m to 390 m. Along these boreholes, the samples are taken with a spacing of 20 m, yielding a regular sampling design of 40 m × 40 m × 20 m. The uniaxial compressive strength (P1) was measured from laboratory tests. Cylindrical rock samples were prepared according to the standard ASTM D4543–08, and then tested under uniaxial compressive conditions using the standards included in ASTM D7012–04. The average prepared sample has an aspect ratio (H/D) of 2. Table 1 presents the average density and the uniaxial compressive strength normalized to a diameter of 50 mm (UCS_{50 mm}) for each lithological unit. The RQD (P2) was estimated directly from borehole logging. To estimate the average discontinuity spacing (P3), the average frequency of fractures (FF/m) was estimated. Bias correction was then applied by considering the average angle of each measured discontinuity. The condition of discontinuities (P4) was not quantitatively measured at the field. A regular condition was assumed for all lithological units. Finally, the water condition (P5) was assigned in agreement to the level of water determined at different depths at each borehole; two classes were mainly identified: *wet* and *damp*.

According to the results of rock mechanics laboratory tests and the interpreted RMR values from the borehole samples, the rock mass is classified with a quality of fair to good (mostly in the range of 50 to 60). This range of RMR values is used in the mine design process. Plan views of the data are shown in Fig. 2.

The RMR simulation should result in a better and improved understanding of the spatial distribution and an easier identification of heterogeneities and uncertainty levels. In addition to RMR, the underlying geomechanical parameters (P1 to P5) could also be mapped and consequently used in numerical models and mine design process in order to obtain a more accurate zoning of the rock mass.

3.1. Exploratory analysis

Basic statistics of the data are presented in Table 2. RMR may vary from 0 to 100, while the values of the parameters P1 to P5 refer to their rating obtained from the application of the RMR system.

According to the data statistics, with a minimum RMR value of 48 and a maximum value of 78, the geomechanical quality of the rock mass varies from fair to good. Concerning the individual parameters (Fig. 3), P1 varies within a short range, meaning that the UCS of the intact rock is almost constant, unlike P2 and P3 that vary in a much wider range showing very different levels of rock mass fracturing. In contrast, for all the samples, the fourth parameter (P4) is constant and equal to 20. This parameter is related to the condition of the discontinuities, so they are all classified as having slightly rough surfaces with a separation smaller than 1 mm and a highly weathered wall rock. Accordingly, the same score (20) will be assumed for all the points of the target simulation grid. Lastly, like P1, parameter P5 varies within a short range, with only two different scores, representing a groundwater condition that is mostly wet (7) and punctually damp (10).

Before performing the simulation of parameters P1, P2, P3 and P5, it is necessary to observe the existing correlations between them, in order to make sure that they are not (or weakly) cross-correlated. Otherwise, the separate parameter simulation in the second approach should be replaced by co-simulation, which would make the model quite more complex (Emery and Cornejo, 2010). The correlation matrix, which contains the Pearson product–moment correlation coefficients between all the parameters, is presented in Table 3. Analyzing these coefficients, one observes that the only parameters with a positive correlation are P3 and P5 comparatively to P2, whereas the others parameters show a slightly negative correlation between them. However, these correlations are rather weak from a statistical point of view (less than 0.3 in absolute value), so that the information on a parameter actually brings little information on the other parameters. The low correlation between P2 (RQD) and P3 (discontinuity spacing) can be explained by the good quality of the rock mass, which translates into a wide spacing of the discontinuities and high RQD values, making the latter parameter less sensitive to closer discontinuities. As such, in Approach 2 the simulation of the four RMR parameters can be performed separately as individual variables; co-simulation, which enhances the simulation of a set of variables in order to reproduce their cross-correlation, is not necessary here.

3.2. Modeling univariate distributions

As previously mentioned, for the first approach, the data should be transformed into normal scores. Since the sampling design is regular,

Table 1
Information about average UCS and average density by lithological unit.

Lithological unit	Description	Average density (t/m ³)	Average UCS (MPa)
Silty and clayey limestone	Medium to fine calcareous sandstone and limestone	2.68 ± 0.05	215 ± 56
Calcareous sandstone	Fine bioclastic calcareous sandstones, limestones and bioclastic clams	2.68 ± 0.09	154 ± 47
Sandstone	Calcareous sandstone with rounded fragments of quartz	2.64 ± 0.02	143 ± 20
Calcareous sandstone	Sandstones with interblended limestones; levels of fine multicolored calcareous sandstones	2.63 ± 0.06	152 ± 40

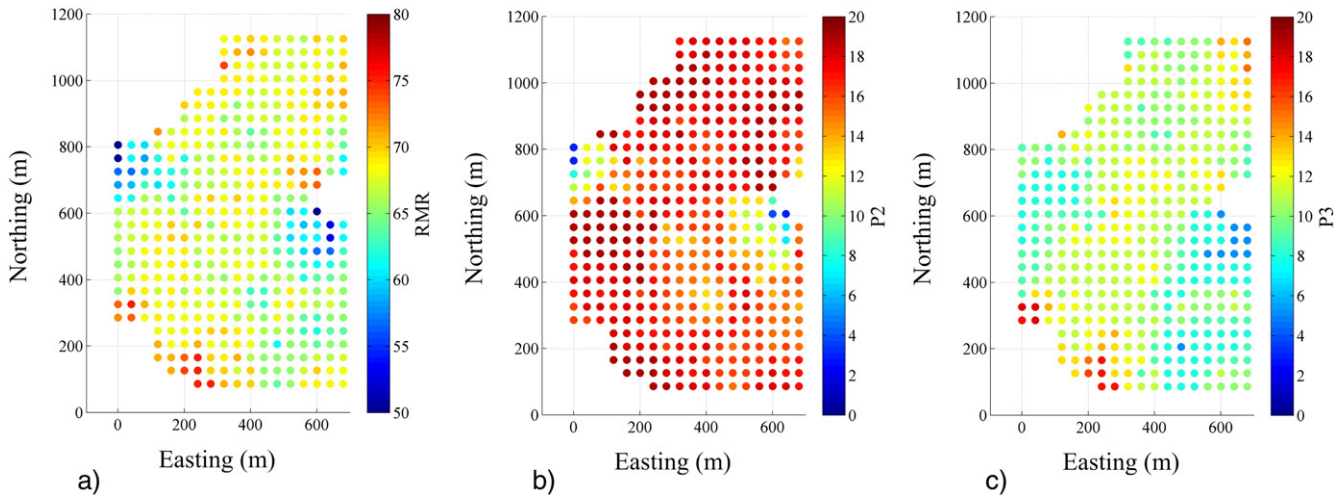


Fig. 2. 2D maps of spatial distribution at elevation 3560 m, for RMR original values (a), Parameter P2 (b) and Parameter P3 (c).

there is no need for declustering, i.e., all the data are assigned the same weighting. The function that relates the original RMR values and the associated Gaussian values (anamorphosis function) can then be calculated empirically with the available data. This function is modeled by using a piecewise linear interpolation between the empirical points, and exponential functions for tail extrapolation, as explained in Emery and Lantuéjoul (2006) (Fig. 4). The parameters of these exponential functions are chosen in order to fit a model as continuous as possible. The absolute minimum and maximum values for RMR are set to 45 and 80, respectively.

Regarding Approach 2, the data related to Parameter 1 only present two different scores, 12 and 14, with relative proportions of 0.468 and 0.532, respectively. This distribution can be modeled by truncating a standard normal distribution, using a single truncation threshold set to $G^{-1}(0.468) = -0.0803$, with G the standard normal cumulative distribution function. In other words, the probability for a standard Gaussian random variable to be less than -0.0803 is 0.468, and the probability to be more than -0.0803 is 0.532, coinciding with the proportions of the two scores of Parameter 1. Likewise, the data of Parameter 5 only assume two different scores, 7 and 10, with relative proportions of 0.989 and 0.011, respectively. Again, the model uses a single truncation threshold, here equal to $G^{-1}(0.989) = 2.2904$.

In a different way, the data of Parameters 2 and 3 assume almost every score. As a result, a larger number of truncation thresholds have to be defined, as shown in Tables 4 and 5, respectively. These truncation thresholds are such that the proportion of data with a given score coincides with the probability for a standard Gaussian random variable to be between the lower and upper thresholds associated with this score.

3.3. Modeling spatial continuity: variogram analysis

For both approaches, following the methodology explained in Section 2, the variograms of the Gaussian random fields to simulate

have to be calculated along the main directions of anisotropy. Because of the sampling design (vertical boreholes), it is not possible to experimentally calculate variograms in inclined directions, thus calculations are restricted to the vertical direction and to the horizontal plane. Furthermore, isotropic variograms are calculated on this plane, insofar as no clear anisotropy is detected in the experimental variograms associated with different horizontal directions. For calculations, the lag distances are multiple of 20 m along the vertical, which corresponds to the data spacing along the boreholes, and of 40 m along the horizontal (borehole spacing), with a tolerance of 20 m.

The experimental variograms (hereafter denoted with the Greek letter γ) so calculated are then fitted using combinations of basic nested structures (exponential, spherical, cubic and Gaussian, see Chilès and Delfiner, 2012 for details on these basic models), as follows.

- Variogram model for Approach 1 (normal score transform of RMR):

$$\gamma = 0.771 \text{ Exponential (250 m; 250 m)} + 0.305 \text{ Gaussian (450 m; 250 m)}$$

- Variogram models for Approach 2:

P1 : $\gamma_1 = 1$ Cubic (700 m; 100 m)

P2 : $\gamma_2 = 1$ Exponential (350 m; 300 m)

P3 : $\gamma_3 = 0.639$ Exponential (300 m; 250 m) + 0.361 Gaussian (300 m; 350 m)

P5 : $\gamma_5 = 0.01$ Exponential (30 m; ∞) + 0.99 Gaussian (700 m; 150 m).

Table 2 Basic statistics on RMR ratings and original data (3969 samples).

	RMR	P1 (UCS)		P2 (RQD)		P3 (JS)		P4 (JC)		P5 (GW)	
		Rating	MPa	Rating	%	Rating	mm	Rating	JC	Rating	GW
Minimum	48.0	12.0	138.0	3.0	0.0	5.0	23.0	20.0	1.0 ^a	7.0	1.0 ^b
Maximum	78.0	14.0	208.0	20.0	100.0	19.0	1923.0	20.0	1.0 ^a	10.0	2.0 ^b
Mean	66.7	13.1	177.8	16.4	87.3	10.2	220.5	20.0	1.0 ^a	7.0	1.0
Standard deviation	3.8	1.0	32.5	2.7	12.3	2.0	170.2	0.0	0.0	0.3	0.1

^a 1.0 was the value used to represent the intermediate rating of the joint condition.
^b 1.0 and 2.0 represent a groundwater condition of Wet and Damp, respectively.

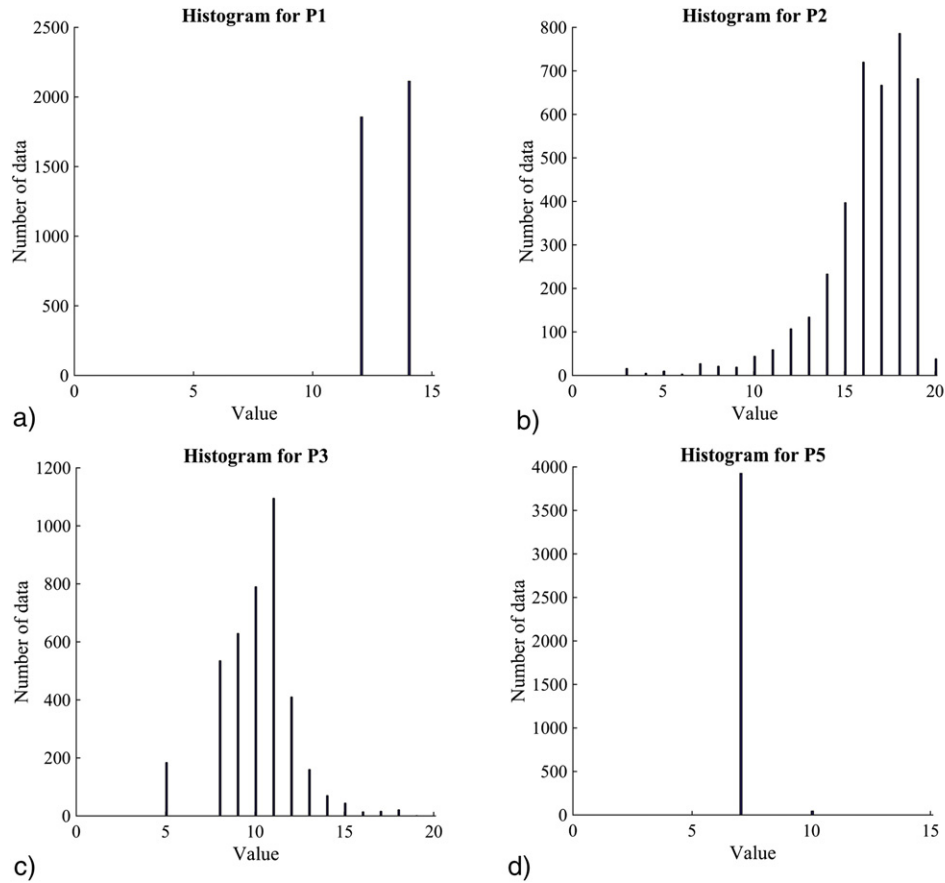


Fig. 3. Data histograms for Parameters P1 (a), P2 (b), P3 (c) and P5 (d).

In the above equations, the coefficient preceding a basic nested structure indicates the sill of this structure (contribution to the total variance), while the distances written between brackets represent the correlation ranges of the structure along the horizontal plane and the vertical direction, respectively. The experimental and theoretical variograms for Approaches 1 and 2 are shown in Figs. 5 and 6, respectively. It should be noticed that none of the variograms exhibit a nugget effect (discontinuity near the origin), indicating that the RMR and its underlying parameters are continuous in space. Even more, the variogram models for P1 and P5 have a smooth behavior near the origin and a large correlation range along the horizontal direction (700 m), which indicates that the regions where these parameters are constant have smooth boundaries and a large spatial extent or spatial connectivity (recall that both P1 and P5 only assume two different scores).

3.4. Conditional simulation results

The model parameters being specified (anamorphosis function in Approach 1, truncation thresholds in Approach 2, and variograms of the underlying Gaussian random fields in both approaches), conditional realizations of the RMR and of the underlying parameters can be constructed. In this work, adaptations of previously published computer

programs are used for simulating Gaussian and truncated Gaussian random fields (Emery and Lantuéjoul, 2006; Emery, 2007). The number of realizations is set to one hundred, so that the post-processing outputs (average and conditional probabilities) could be calculated with a reasonable approximation. In both cases, the turning bands algorithm is applied with 1000 turning lines to generate the Gaussian random fields, and simple kriging is used to condition the realizations to the borehole data. For Approach 2, the Gibbs sampler is stopped after one hundred

Table 3
Correlation matrix between parameters P1, P2, P3 and P5.

	P1	P2	P3	P5
P1	1	-0.096	-0.164	-0.113
P2	-0.096	1	0.292	0.045
P3	-0.164	0.292	1	-0.032
P5	-0.113	0.045	-0.032	1

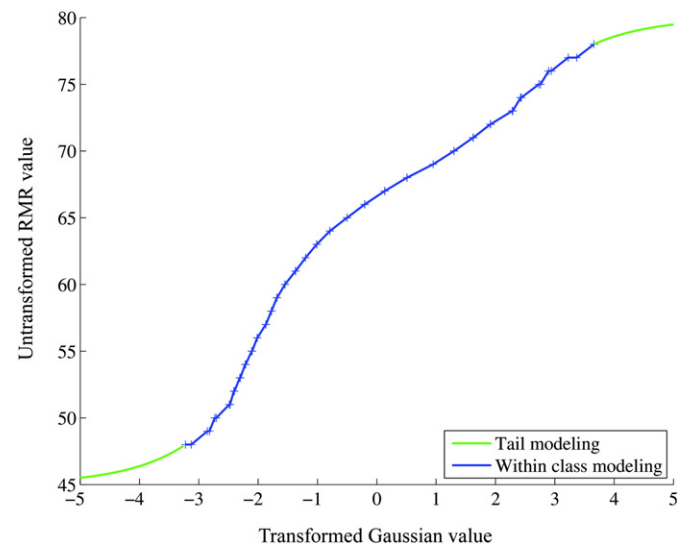


Fig. 4. Anamorphosis function used for Approach 1. The ordinate indicates the RMR value and the abscissa the associated Gaussian value.

Table 4
Calculated proportions for P2 data with the corresponding Gaussian thresholds.

Score for P2	Cumulative proportion	Lower threshold	Upper threshold
1	0	−∞	−∞
2	0	−∞	−∞
3	0.0033	−∞	−2.7164
4	0.0043	−2.7164	−2.6276
5	0.0073	−2.6276	−2.4422
6	0.0080	−2.4422	−2.4089
7	0.0150	−2.4089	−2.1701
8	0.0200	−2.1701	−2.0537
9	0.0250	−2.0537	−1.9600
10	0.0360	−1.9600	−1.7991
11	0.0510	−1.7991	−1.6352
12	0.0780	−1.6352	−1.4187
13	0.1120	−1.4187	−1.2160
14	0.1710	−1.2160	−0.9502
15	0.2710	−0.9502	−0.6098
16	0.4520	−0.6098	−0.1206
17	0.6200	−0.1206	0.3055
18	0.8180	0.3055	0.9078
19	0.9900	0.9078	2.3263
20	1.0000	2.3263	+∞

iterations and the simulated Gaussian random fields are truncated, based on the thresholds indicated in Section 3.2 and Tables 4 and 5, yielding realizations of parameters P1 to P5 that are subsequently summed to obtain realizations of the RMR values.

For ease of display, the locations targeted for simulation correspond to a regular two-dimensional grid placed at elevation 3560 m, with a mesh of 5 m × 5 m and a total of 160 nodes along the east direction and 240 nodes along the north direction.

The average of the RMR realizations is calculated to map the expected RMR over the region of interest resulting from both approaches (Fig. 7b, e). Furthermore, in order to demonstrate the spatial variability existing in this rock mass, the first realization is mapped as an example (Fig. 7a, d). In these figures, the neighboring data values are superimposed on the maps in order to highlight the effect of conditioning the RMR realizations to the borehole data: when a target grid node coincides with a data location, the simulated RMR value exactly matches the conditioning data value.

The visual comparison suggests that the two approaches produce similar results for RMR. It is worth noticing that the map of the realization average tends to smudge the contrasts and that spatial heterogeneities appear as much more faded. The analysis of the individual realizations is therefore important to visualize the real heterogeneity

Table 5
Calculated proportions for P3 with the corresponding Gaussian thresholds.

Score for P3	Cumulative proportion	Lower threshold	Upper threshold
1	0	−∞	−∞
2	0	−∞	−∞
3	0	−∞	−∞
4	0	−∞	−∞
5	0.0500	−∞	−1.6449
6	0.0501	−1.6449	−1.6439
7	0.0502	−1.6439	−1.6429
8	0.1842	−1.6429	−0.8995
9	0.3432	−0.8995	−0.4037
10	0.5422	−0.4037	0.1060
11	0.8152	0.1060	0.8972
12	0.9182	0.8972	1.3931
13	0.9582	1.3931	1.7302
14	0.9762	1.7302	1.9809
15	0.9872	1.9809	2.2322
16	0.9912	2.2322	2.3739
17	0.9952	2.3739	2.5899
18	0.9998	2.5899	3.5401
19	1.0000	3.5401	+∞
20	1.0000	+∞	+∞

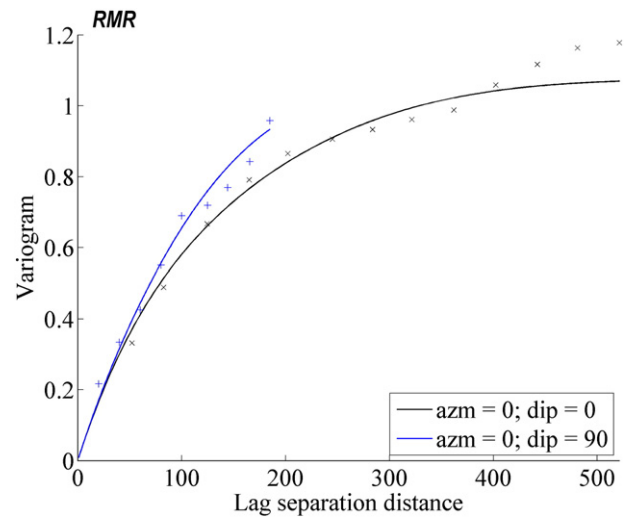


Fig. 5. Experimental (crosses) and theoretical (solid lines) variograms for RMR (Approach 1) along the main anisotropy directions: horizontal (black) and vertical (blue).

that it is expected to be observed in the field, whereas the average of the realizations shows an overall trend, which is much smoother.

3.5. Post-processing simulations

More outputs can be represented, like the probability that the RMR exceeds or falls short of a predefined value, which can be estimated by the frequency of threshold exceedance or non-exceedance observed over the realizations. This representation is of great value if one wants to identify regions where very high or low geomechanical properties could be present, and with which probability. As an example, for both approaches, Fig. 8 shows the map of the probability that the actual RMR is less than a threshold of 65.

Fig. 9 (a, b, d, e) shows the maps of parameters P2 and P3 for the first realization and for the average of 100 realizations obtained with Approach 2, which helps to visualize the spatial distribution and variability of the discontinuity parameters. Comparing realization #1 with the average of 100 realizations for both parameters, the pattern in lower or higher rating are similar, however, as already referred, the average mapping exhibits smoother values. The individual analysis of the discontinuity parameters can, by itself, result in a powerful tool in geotechnical works to understand the regions where the rock mass can be more or less fractured. Attentively, comparing the P2 and P3 maps (average and first realization), it is possible to identify a small region in the western part of the grid, with low values of RQD (P2) and intermediate values of the discontinuity spacing (P3). These incoherent values are actually present in the borehole data used for conditioning the realizations, therefore they are not a problem of the proposed simulation approach, but rather a problem of the input data. This could be explained by human errors in the measurement of parameter P2.

Maps of other geomechanical parameters can be obtained based on the realizations of RMR. In this work, considering that the RMR values are higher than 50, the distribution maps of the deformation modulus (E_m) were developed with the Bieniawski (1978) empirical formula:

$$E_m = 2 \times RMR - 100.$$

This formula uses the simulated values of RMR to obtain the E_m values at the same locations. Alike the maps computed for the RMR values, Fig. 10 (a, b) shows the average of E_m obtained from the 100 conditional realizations of Approach 1, as well as the first realization, as an

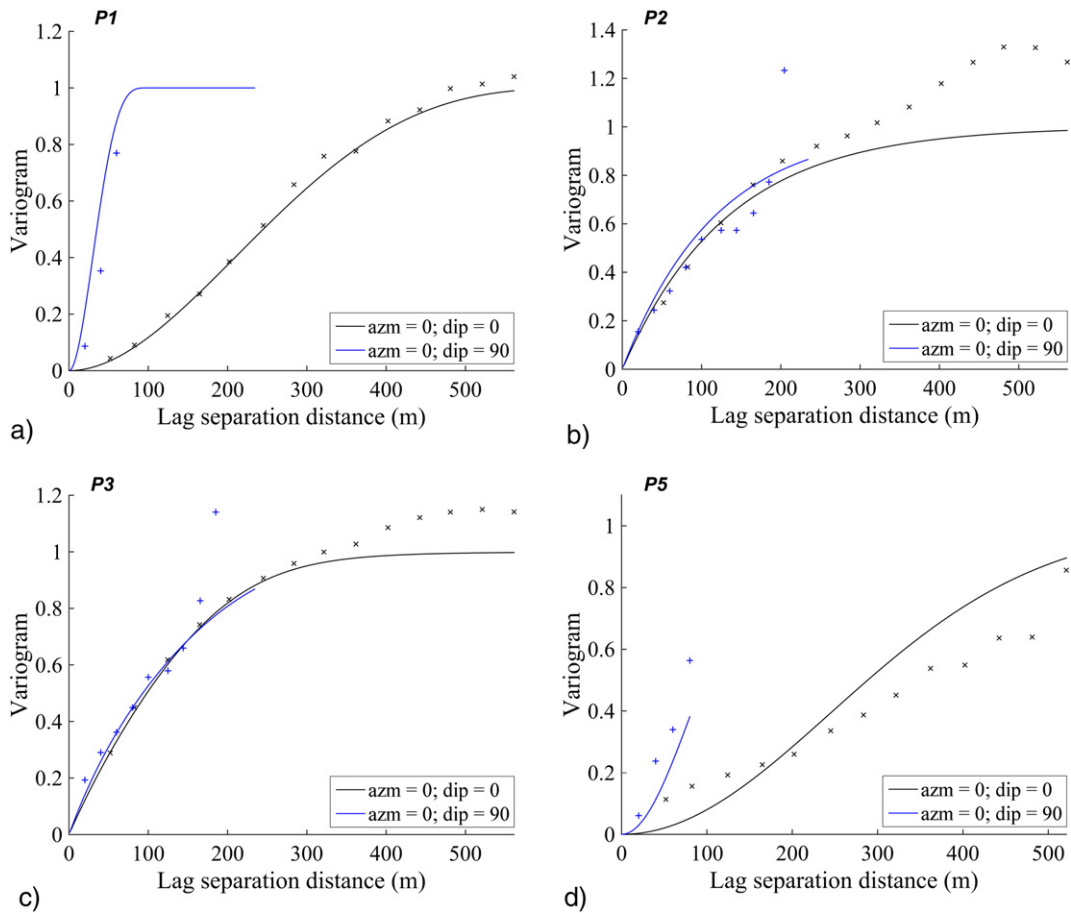


Fig. 6. Experimental (crosses) and theoretical (solid lines) variograms for Approach 2 along the main anisotropy directions: horizontal (black) and vertical (blue): Parameters P1 (a), P2 (b), P3 (c) and P5 (d).

example. With this map it is possible to distinguish zones where the rock mass is significantly stiffer and zones with lower rigidity.

Finally, to visualize the uncertainty in the true values, the standard deviation (or any other uncertainty measure, such as the coefficient of variation or the limits for a given level of confidence) can be calculated at each target node over the 100 realizations and mapped throughout the grid of interest. As an example, the standard deviations of RMR obtained with both approaches, of parameters P2 and P3 obtained in the truncated Gaussian model (Approach 2) and of the deformation modulus E_m obtained in the multi-Gaussian model (Approach 1) are mapped in Fig. 7 (c, f), Fig. 9 (c, f) and Fig. 10 (c), respectively. Such maps indicate how much the true unknown values are likely to deviate from their expected values (averages of the realizations) at each target grid node, therefore quantify the local uncertainty in the true values. The mapped standard deviations depend on the number and location of the surrounding borehole data (they increase in under-sampled areas and peripheral areas without data) and, to a lesser extent, on the parameter values: for P3, whose distribution is positively skewed, the standard deviation tends to increase in high-valued areas, while the reverse happens for RMR, P2 and E_m whose distributions are negatively skewed, a phenomenon known as proportional effect (Manchuk et al., 2009) or regressive effect (David, 1988). Furthermore, the maximum standard deviation for RMR occurs in the north-western side of the grid of interest and is about 7 (Fig. 7), which represents a small deviation for a variable that varies from 0 to 100. This suggests a relatively low uncertainty in the true RMR values at unsampled locations.

The standard deviations mapped in Figs. 7, 9 and 10 should not be confused with the ones presented in Table 2: the former measure the variability across the realizations at a given location, therefore depend on the location under consideration, whereas the latter measure the

variability of a data set across the region of interest, without distinguishing any specific location.

3.6. Split-sample cross-validation

To validate the two approaches the original data set is randomly divided into two subsets, each containing one half of the data. Thereby, the first subset (training subset) is used to simulate the RMR at the locations of the data belonging to the second subset (validation subset).

In order to validate the prediction capability of both approaches, the expected RMR, calculated as the average of the simulated RMR values, is compared with the real values at the locations of the validation subset (Fig. 11a, b). To analyze the results, a linear regression and the coefficient of determination between expected and true RMR values are calculated. For both approaches, the resulting points of the scatter plot are distributed close to the diagonal line and the coefficient of determination is high (0.788 and 0.771, respectively, for Approaches 1 and 2). This indicates that the simulations allow an accurate prediction of RMR, with small error fluctuation and no conditional bias (Chilès and Delfiner, 2012). Accuracy can be confirmed by calculating the Root Mean Squared Error (RMSE):

$$RMSE = \sqrt{\frac{\sum_{i=1}^N (y_i - \hat{y}_i)^2}{N}} \quad (1)$$

where N denotes the number of data in the validation subset, y_i the true value and \hat{y}_i the expected value (average of the realizations). The RMSE values are 1.74 for Approach 1 and 1.81 for Approach 2. Since RMR varies from 0 to 100, an error less than 2 is almost residual.

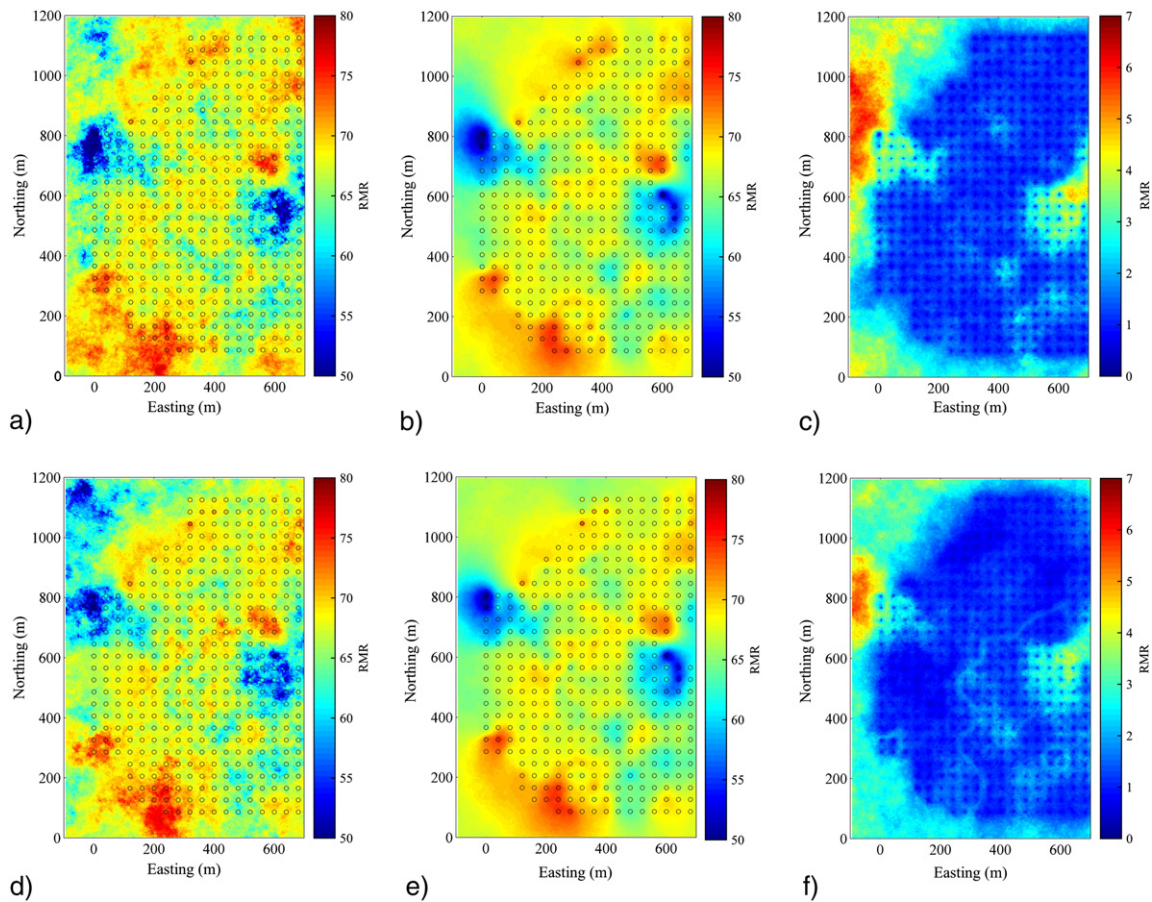


Fig. 7. Maps of RMR at elevation 3560 m, for realization #1 (a, d), average of 100 realizations (b, e), standard deviation of 100 realizations (c, f), obtained with Approach 1 (a, b, c) and Approach 2 (d, e, f).

In order to validate the capability of modeling uncertainty, accuracy plots (Goovaerts, 2001) are constructed. In these plots, one considers a given probability p and, based on the obtained realizations, one can define at each target location an interval with such a probability (the interval bounds are the quantiles $1-p/2$ and $1 + p/2$ of the set of simulated values). Subsequently, the location is assigned a value of 1 if the true RMR belongs to the interval and 0 otherwise. It is expected that, on average over all the locations of the validation subset, the proportion of 1 should be close to the probability p under consideration. This procedure has been applied with p varying from 0 to 1 (Fig. 11c, d). In both

approaches, the observed proportion is close to the theoretical probability (points close to the diagonal line, with a slightly better coincidence for Approach 2), indicating that the realizations accurately assess the uncertainty in the actual RMR values.

3.7. Discussion

Both simulation approaches give an insight into two characteristics of the geomechanical parameters of interest: (1) their heterogeneity at all spatial scales, especially at short scale, which can be assessed on

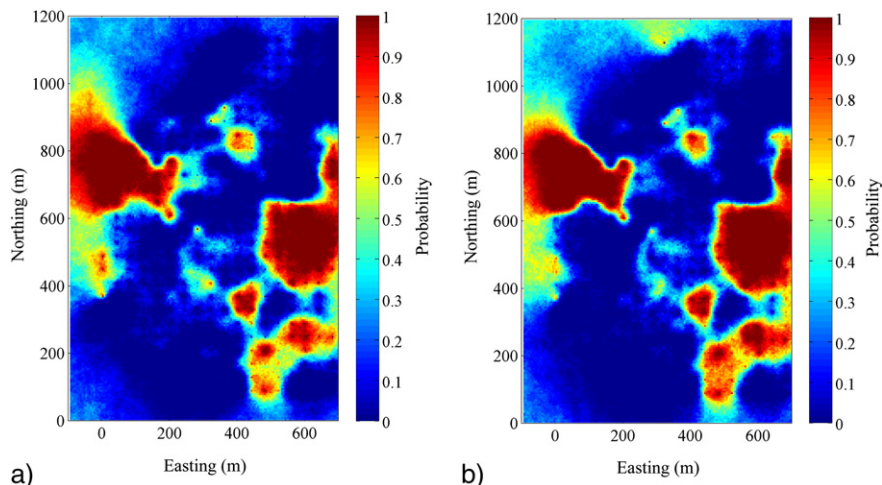


Fig. 8. Maps of probability (between 0 and 1) that the RMR is less than a threshold of 65 at elevation 3560 m, obtained with Approach 1 (a) and Approach 2 (b).

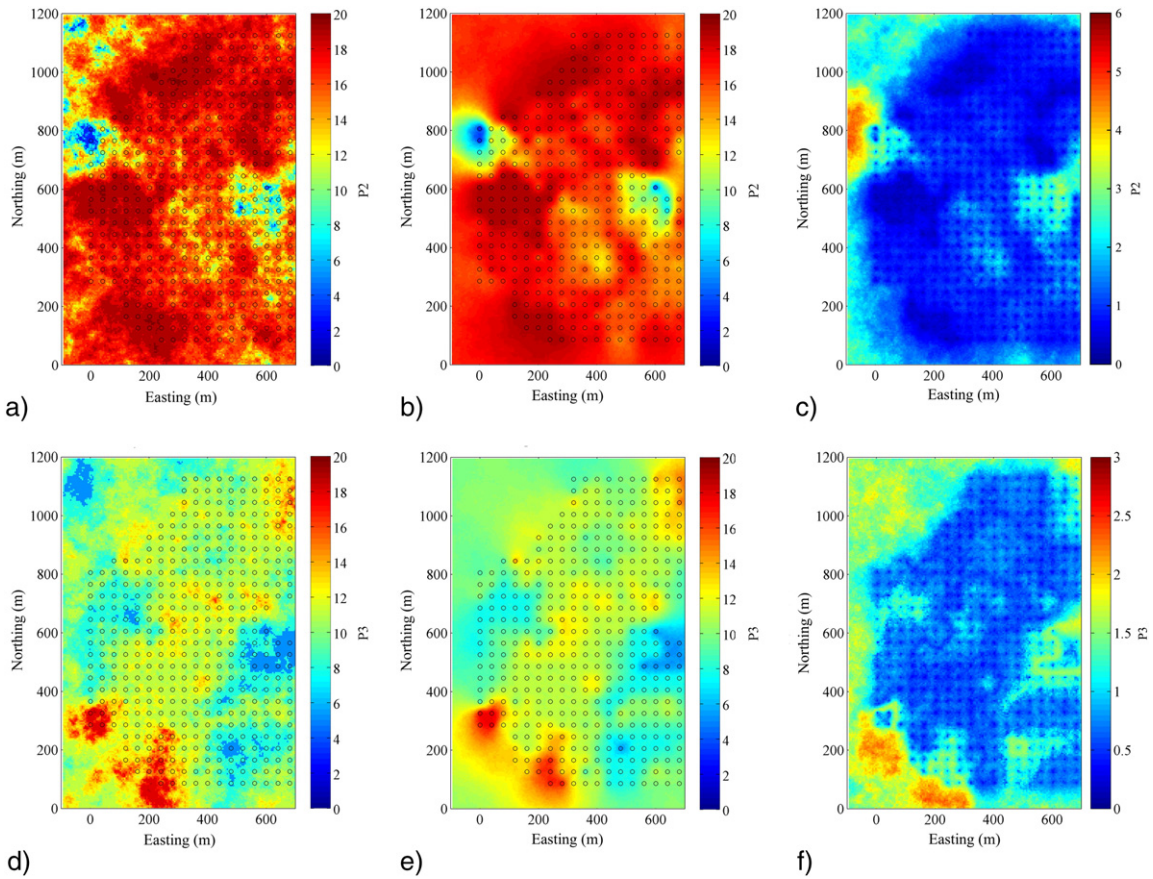


Fig. 9. Maps of discontinuity parameters at elevation 3560 m, for realization #1 of P2 (a), average of 100 realizations of P2 (b), standard deviation of 100 realizations of P2 (c), realization #1 of P3 (d), average of 100 realizations of P3 (e), and standard deviation of 100 realizations of P3 (f).

each individual realization; and (2) the uncertainty in the true values at unsampled locations. The latter can be assessed by comparing a set of realizations at the same location or jointly over several locations, e.g., by calculating the standard deviation of the realizations at each location, which measures how much the true unknown values may deviate from their expected values (average of the realizations).

There are several differences between these two proposed approaches, mainly regarding pre and post processing. While Approach 1 allows directly simulating the RMR as a continuous variable, the quantity and detail of the geomechanical information is more limited when compared with Approach 2 that allows the simulation of the parameters

underlying the definition of RMR. Also, the difference in modeling and computational efforts for both approaches is substantial, Approach 1 being a faster and simpler alternative than Approach 2. Regarding the results, the observed differences are generally not significant when mapping one realization or the average of a set of realizations, but differences are perceptible when mapping the standard deviations of the realizations: Approach 2 yields a lower standard deviation (reflecting less uncertainty) than Approach 1 in the peripheral zones. All things considered, the choice of the best approach should be made based on the resources and needs of the practitioner (degree of required geotechnical detail, understanding of the models, software and time availability).

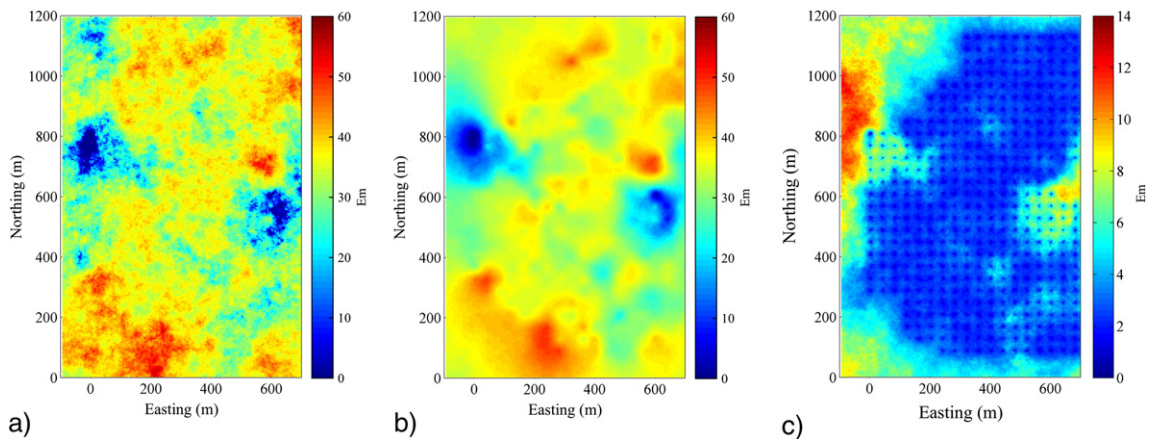


Fig. 10. Maps of deformation modulus (GPa) at elevation 3560 m, for realization #1 (a), average of 100 realizations (b), standard deviation of 100 realizations (c), obtained with Approach 1.

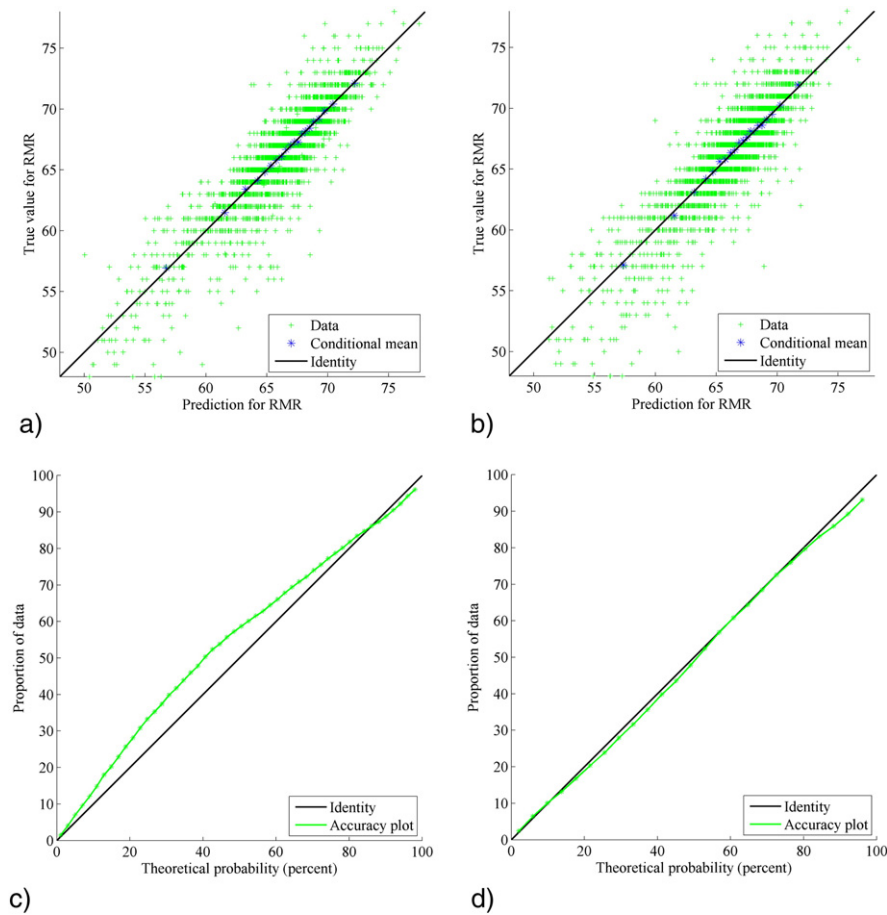


Fig. 11. Cross-validation results: scatter plots between true and expected RMR values (a, b), and accuracy plots (c, d) for Approach 1 (a, c) and Approach 2 (b, d).

4. Conclusions

This paper presented two geostatistical approaches for simulating RMR. The first one considers the direct simulation of RMR, viewed as a variable measured on a continuous scale, while the second one separately simulates the underlying parameters constituting the RMR system (viewed as variables measured on a discrete scale). Both approaches lead to similar results in terms of expected RMR and processed outputs. According to the split-sample validation technique, both have a good performance in terms of prediction accuracy and measurement of uncertainty, which makes them viable for RMR modeling.

The first approach presents the advantage of needing a lower computation and pre-processing time, maintaining a good predictive accuracy, which is an interesting feature from a practical implementation point of view. On the other hand, even though with higher computational costs needed for its implementation, the second approach presents a slightly higher accuracy and provides information on the RMR individual parameters, which is useful for geotechnical analyses. For example, the simulation of parameters P2 and P3, which are related with the fracturing of the rock mass, can provide an overview about the regions where a higher permeability is expected. Furthermore, since it simulates variables measured on discrete scales, this second approach is consistent with the nature of the geomechanical parameters to be modeled, which are ratings rather than variables defined on a continuous scale. If these parameters were cross-correlated, they should be jointly simulated in order to reproduce such cross-correlations.

The two proposed approaches prove that individual realizations are much more accurate in defining the heterogeneities at short scale, while the average of the realizations tends to smooth these heterogeneities.

Besides the mapping of the expected RMR and underlying parameters, the realizations allow mapping probabilities that show if the true values are above or below a defined threshold. In addition, the standard deviation can also be mapped indicating if true parameters fluctuate around their expected values. Those maps are very helpful to quantify risks and uncertainties at any target location (or group of locations) in space. By applying empirical formulas, one can also map the deformation modulus (E_m) as a function of the RMR. Together with other parameters like GSI and Q, these maps can be used to develop numerical models that explicitly consider the heterogeneities at all spatial scales, providing a more accurate understanding of the rock mass behavior than traditional interpolation approaches.

Acknowledgments

This research was funded by the Portuguese Foundation for Science and Technology (FCT), through ISISE project UID/ECI/04029/2013, by the Chilean Economic Development Agency (CORFO), through Project Innova Chile—CORFO 11IDL2-10630, and by the Chilean Commission for Scientific and Technological Research (CONICYT), through Projects CONICYT/FONDECYT/REGULAR/N°1130085 and CONICYT PIA Anillo ACT 1407. The authors are grateful to four anonymous reviewers for their constructive comments.

References

- Armstrong, M., Galli, A., Beucher, H., Le Loc'h, G., Renard, D., Doligez, B., Eschard, R., Geffroy, F., 2011. *Plurigaussian Simulations in Geosciences*. second ed. Springer, Berlin, p. 176.

- Bieniawski, Z.T., 1978. Determining rock mass deformability: experience from case histories. *Int. J. Rock Mech. Mining Sci.* 15, 237–247.
- Bieniawski, Z.T., 1989. *Engineering rock mass classifications: a complete manual for engineers and geologists in mining, civil, and petroleum engineering*. Wiley, New York, USA, p. 272.
- Chilès, J.P., Delfiner, P., 2012. *Geostatistics: modeling spatial uncertainty*. Wiley, New York.
- David, M., 1988. *Handbook of Applied Advanced Geostatistical Ore Reserve Estimation*. Elsevier, Amsterdam.
- Deisman, N., Khajeh, M., Chalaturnyk, R.J., 2013. Using geological strength index (GSI) to model uncertainty in rock mass properties of coal for CBM/ECBM reservoir geomechanics. *Int. J. Coal Geol.* 112, 76–86.
- Deutsch, C.V., Journel, A.G., 1998. *GSLIB: geostatistical software library and user's guide*. Oxford University Press, Oxford.
- Egaña, M., Ortiz, J., 2013. Assessment of RMR and its uncertainty by using geostatistical simulation in a mining project. *J. GeoEng.* 8 (3), 83–90.
- Ellefmo, S.L., Eidsvik, J., 2009. Local and spatial joint frequency uncertainty and its application to rock mass characterisation. *Rock Mech. Rock. Eng.* 42 (4), 667–668.
- Emery, X., 2007. Simulation of geological domains using the plurigaussian model: new developments and computer programs. *Comput. Geosci.* 33 (9), 1189–1201.
- Emery, X., Cornejo, J., 2010. Truncated Gaussian simulation of discrete-valued, ordinal coregionalized variables. *Comput. Geosci.* 36 (10), 1325–1338.
- Emery, X., Lantuéjoul, C., 2006. TBSIM: a computer program for conditional simulation of three-dimensional Gaussian random fields via the turning bands method. *Comput. Geosci.* 32 (10), 1615–1628.
- Esfahani, N.M., Asghari, O., 2013. Fault detection in 3D by sequential Gaussian simulation of Rock quality designation (RQD). *Arab. J. Geosci.* 12 (10), 3737–3747.
- Exadaktylos, G., Stavropoulou, M., 2008. A specific upscaling theory of rock mass parameters exhibiting spatial variability: analytical relations and computational scheme. *Int. J. Rock Mech. Mining Sci.* 45, 1102–1125.
- Ferrari, F., Apuani, T., Giani, G.P., 2014. Rock mass rating spatial estimation by geostatistical analysis. *Int. J. Rock Mech. Mining Sci.* 70, 162–176.
- Goovaerts, P., 2001. Geostatistical modeling of uncertainty in soil science. *Geoderma* 103, 3–26.
- Jeon, S., Hong, C., You, K., 2009. Design of tunnel supporting system using geostatistical methods. In: Huang, Liu (Ed.), *Geotechnical Aspects of Underground Construction in Soft Ground*, pp. 781–784.
- Journel, A.G., 1974. Geostatistics for conditional simulation of orebodies. *Econ. Geol.* 69 (5), 673–687.
- Lantuéjoul, C., 2002. *Geostatistical simulation, models and algorithms*. Springer, Berlin, p. 256.
- Manchuk, J.G., Leuangthong, O., Deutsch, C.V., 2009. The proportional effect. *Math. Geosci.* 41 (7), 799–816.
- Matheron, G., 1971. The theory of regionalized variables and its applications. *Ecole Nationale Supérieure des Mines de Paris, Fontainebleau*, p. 211.
- Oh, S., Chung, H., Kee Lee, D., 2004. Geostatistical integration of MT and boreholes data for RMR evaluation. *Environ. Geol.* 46, 1070–1078.
- Ozturk, C.A., Nasuf, E., 2002. Geostatistical assessment of rock zones for tunneling. *Tunn. Undergr. Space Technol.* 17, 275–285.
- Ozturk, C.A., Simdi, E., 2014. Geostatistical investigation of geotechnical and constructional properties in kadikoy–kartal subway. *Turk. Tunn. Undergr. Space Technol.* 4, 35–45.
- Rosenbaum, M.S., Rosen, L., Gustafson, G., 1997. Probabilistic models for estimating lithology. *Eng. Geol.* 47, 43–55.
- Ryu, D.W., Kim, T.K., Heo, J.S., 2003. A study on geostatistical simulation technique for the uncertainty modeling of RMR. *Tunn. Undergr.* 13, 87–99 (in Korean with English abstract).
- Stavropoulou, M., Exadaktylos, G., Saratsis, G., 2007. A combined three-dimensional geological-geostatistical numerical model of underground excavations in rock. *Rock Mech. Rock. Eng.* 40 (3), 213–243.
- You, K.H., 2003. An estimation technique of rock mass classes for a tunnel design. *Korean Geotech. Eng.* 19 (5), 319–326 (in Korean with English abstract).